Acta Crystallographica Section B
Structural Science
ISSN 0108-7681

Simulated annealing structure solution of a new phase of dicalcium silicate Ca_2SiO_4 and the mechanism of structural changes from α-dicalcium silicate hydrate to α_L'-dicalcium silicate *via* the new phase

H. Toraya[a]* and S. Yamazaki[b]

[a]Ceramics Research Laboratory, Nagoya Institute of Technology, Asahigaoka, Tajimi 507-0071, Japan, and [b]Basic Research Center, INAX Corporation, Tokoname, Aichi 479-0848, Japan

Correspondence e-mail: toraya@crl.nitech.ac.jp

Received 7 January 2002
Accepted 20 March 2002

A new phase of dicalcium silicate (Ca_2SiO_4) was formed by heating α-dicalcium silicate hydrate [α-$Ca_2(SiO_4H)OH$ = α-C_2SH] at temperatures of ~663–763 K, and it was transformed into α_L'-Ca_2SiO_4 (= α_L'-C_2S) above ~1193 K. The crystal structure of the new phase (hereafter called x-C_2S) has been determined by simulated annealing and refined by the Rietveld method using synchrotron radiation powder diffraction data. The structure consists of isolated SiO_4 tetrahedra and a three-dimensional CaO_n polyhedral network, forming a new structural type of dicalcium silicate. A structural change from α-C_2SH to x-C_2S is compelled by large displacements of SiO_4 tetrahedra, accompanied by dehydration, in the direction perpendicular to the two-dimensional $Ca(O,OH)_n$ polyhedral network in α-C_2SH. With increasing temperature, sizes of CaO_n polyhedra in x-C_2S become too large to confine Ca atoms at the sixfold to eightfold coordination sites. Then the structure of x-C_2S is transformed into α_L'-C_2S, having eightfold to tenfold coordination sites for the Ca atoms.

1. Introduction

Dicalcium silicates Ca_2SiO_4 (hereafter abbreviated C_2S) have been known to have five polymorphs, designated by using the symbols α, α_H', α_L', β and γ in order of decreasing temperature for thermal stability (Eysel & Hahn, 1970) (Fig. 1). The γ-form is stable at room temperature, whereas it is inactive against hydration. The β-form is unstable at room temperature without stabilization with additives or controlling particle size (Kriven, 1988). However, the β-form has hydration activity at room temperature, and it is a very important constituent of Portland cement. These polymorphs constitute, in general, a complicated phase system, and phase relationships, hydration properties, dusting phenomena *etc*. of these polymorphs have been very important subjects of studies in cement technologies. Crystal structures of individual phases and the transformation mechanism from one phase to another have been analyzed by many researchers (Midgley, 1952; Smith *et al.*, 1965; Jost *et al.*, 1977; Udagawa & Urabe, 1978; Catti *et al.*, 1984; Il'inets & Bikbau, 1990), and they have been extensively discussed in cement chemistry as well as in mineralogy and crystallography (Eysel & Hahn, 1970; Udagawa, 1980; Mumme *et al.*, 1995).

Ishida *et al.* (1993) reported the formation of a new phase of dicalcium silicate during the dissociation process of α-$Ca_2(SiO_4H)OH$ (α-C_2SH) at temperatures of ~663–763 K (Fig. 1). This new phase, preliminarily designated x-C_2S, can be stable at room temperature, and it has hydration activity. The new phase can be transformed into α_L'-C_2S by elevating the temperature to 1193–1233 K and further transformed into

β-C_2S on subsequent cooling. Unit-cell parameters and a space group of x-C_2S were determined by our group using synchrotron radiation powder diffraction data (Miyazaki *et al.*, 1998). The unit-cell dimensions of x-C were much closer to those of α-C_2SH than to those of the α'_L-, β- and γ-forms. Moreover, there was no discernible change in shape of the plate-like crystalline particles observed by the scanning electron microscope during the dissociation process from α-C_2SH to x-C_2S. Therefore, the crystal structure of x-C_2S was expected to be similar to that of α-C_2SH. Because of the low crystallinity of the x-C_2S sample formed *via* hydrothermal and heating processes, the powder diffraction pattern could not be well resolved, and no structural solution has been obtained in spite of several trials to solve the crystal structure.

In the present study, the crystal structure of x-C_2S is determined using simulated annealing as a global minimization technique (Kirkpatrick *et al.*, 1983) and synchrotron radiation powder diffraction data used in the previous study (Miyazaki *et al.*, 1998). The present study is expected to be useful for understanding the structural relationships of dicalcium silicates and dicalcium silicate hydrates.

2. Experimental

A brief description of the experimental procedures, given below, may be useful for readers, although detailed descriptions are given by Miyazaki *et al.* (1998).

A powder specimen of x-C_2S was prepared by heating a powder of α-C_2SH at a temperature of 1073 K for 1 h in air.

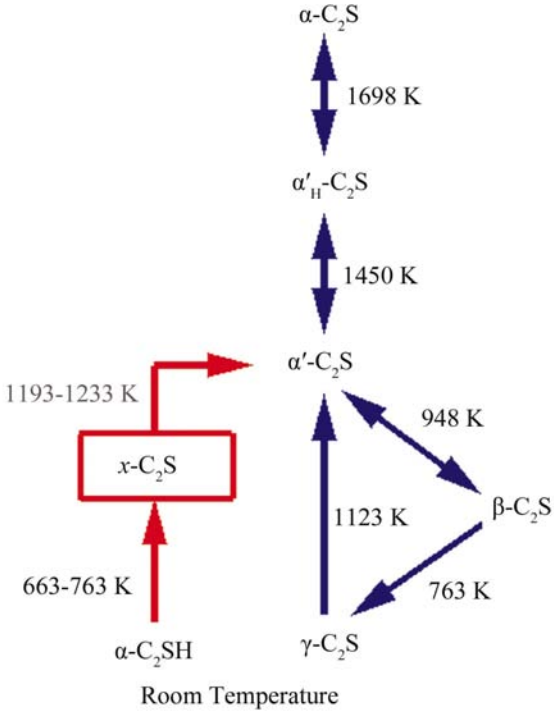

Figure 1
Phase relationship of the present new phase with the established C_2S system. Temperatures of the phase transitions and dissociation were those given by Kriven (1988) and Ishida *et al.* (1993), respectively.

Profile intensities were collected in the 2θ range 8–155° (a step interval of 0.005°) by using a powder diffractometer with a multiple detector system (MDS) (Toraya *et al.*, 1996) and monochromated synchrotron radiation [λ = 1.598 (1) Å] at the beamline BL-4B$_2$ of the Photon Factory in Tsukuba, Japan. An asymmetric 2θ-scan mode at a fixed incident angle of 8° was employed in flat-specimen reflection geometry. The observed profile intensities were corrected for the decay of the incident beam of synchrotron radiation by using the intensities of an incident-beam monitor counter. Therefore, real intensity counts were scaled by a factor ranging from 0.82 to 1.22.

The powder diffraction pattern on the low-angle side was first decomposed by the computer program *PRO-FIT* (version 3.00) for individual profile fitting (Toraya, 1986). The first 21 reflections thus resolved were used for automatic indexing using the computer program *ITO* (Visser, 1969). A unique solution of a monoclinic unit cell with dimensions of a = 8.213, b = 9.806, c = 9.793 Å and β = 94.8° was derived at a figure-of-merit of 20.3. The unit-cell dimensions were well in accordance with those recorded on the $h0l$ reciprocal lattice plane with a selected-area electron diffraction technique (JEOL, JEM2000-FX).

The whole diffraction pattern was decomposed using the computer program *WPPF* (version 3.00) for the whole-powder-pattern decomposition method based on the Pawley algorithm (Toraya, 1986; Pawley, 1981). Observed intensities of powder diffraction lines and those of selected-area electron diffraction spots on the $h0l$ plane were examined. Systematic absences of reflections having indices of $h0l$ with $l = 2n + 1$ (n: integer) and $0k0$ with $k = 2n + 1$ were observed, and a space group of $P2_1/c$ was uniquely derived. Powder diffraction data (d-spacing, integrated intensities and hkl indices) of x-C_2S are reported by Yamazaki & Toraya (2001).

The unit-cell parameters of x-C_2S were refined by using the *WPPF* and laboratory X-ray data (strictly monochromated Cu $K\alpha_1$ radiation) of a sample mixed with National Institute of Standards and Technology (NIST) Standard Reference Material (SRM) 640*b* Si powder (Rasberry, 1987) as an internal standard reference material. Crystallographic data of the x-C_2S are given in Table 1.

3. Structure determination

Powder diffraction lines were all broadened, giving a full width at half-maximum (FWHM) of 0.093–1.60° in the 2θ range 10–150°. In the least-squares fitting for whole-powder-pattern decomposition, neighbouring reflections within an angular distance of 0.4 × FWHM were grouped together in order to avoid strong parameter correlation and parameter divergence. In this case, 94% of reflections in the whole 2θ range must be equi-partitioned (see also Fig. 2 shown later). Therefore, application of direct methods was inadequate for solving the crystal structure of x-C_2S, and simulated annealing as a global minimization technique (Kirkpatrick *et al.*, 1983) was employed instead. The computer program *DSS* (Version 1.00) was recently written by one of the authors (HT) for direct-space search using Monte Carlo methods and simulated

Table 1
Experimental details (Yamazaki & Toraya, 2001).

Crystal data	
Chemical formula	Ca_2SiO_4
Chemical formula weight	172.24
Cell setting, space group	Monoclinic, $P2_1/c$
a, b, c (Å)	8.2127 (5), 9.7930 (4), 9.7954 (5)
β (°)	94.848 (5)
V (Å^3)	785.00 (7)
Z	8
D_x (Mg m^{-3})	2.91
Radiation type	Synchrotron
Wavelength (Å)	1.598
Temperature (K)	298

annealing, and it was used for the present study. Details of *DSS* will be reported elsewhere.

The x-C_2S contains 16 Ca atoms and eight SiO_4 tetrahedra in a unit cell (Table 1). Moreover, an atomic ratio of Si:O = 1:4 in the chemical composition and knowledge about crystal structures of family minerals indicated that the eight SiO_4 tetrahedra are isolated from each other. The space group $P2_1/c$ has special equivalent positions ($2a$ to $2d$) only at the centre of symmetry, whereas the atomic configuration of the SiO_4 tetrahedron is not centrosymmetric. Therefore, it was reasonable to assume that two SiO_4 tetrahedra in an asymmetric unit occupy general equivalent positions ($4e$) in the unit cell. This assumption was well in accordance with nuclear magnetic resonance (NMR) observations, which exhibited two sharp spectral lines indicating the presence of the two kinds of SiO_4 tetrahedra in the unit cell (Ishida *et al.*, 1993).

The possibility that Ca atoms occupy special equivalent positions could not be excluded in the first place. The presence of the Ca atom at the centre of symmetry is, however, only the case in γ-C_2S among the members of the C_2S family (Czaya, 1971). Moreover, it was much more probable that the symmetry of CaO_n polyhedra (where n is the number of coordinated O atoms) in x-C_2S was degraded from the centrosymmetric CaO_6 or CaO_8 polyhedral shape. Therefore, it was first assumed that the four Ca atoms in the asymmetric unit also occupy the general equivalent positions.

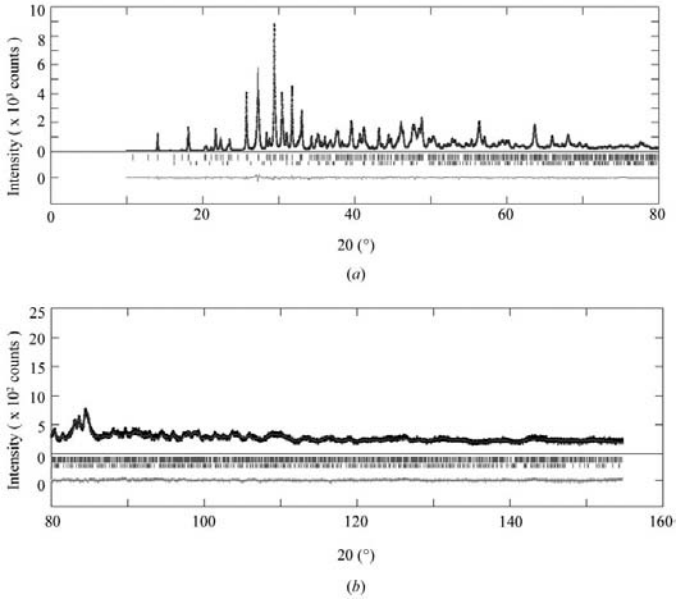

Figure 2
Fitting result of Rietveld refinement for x-C_2S. Filled squares and solid lines represent the observed and calculated profile intensities, respectively. Plots at the bottom of the diagram represent weighted difference plots by $w_i^{1/2}(Y_{oi} - Y_{ci})$. Short vertical bars represent Bragg reflection positions of x-C_2S (upper) and β-C_2S (lower). The latter half of the pattern is presented on an enlarged scale.

The starting model for the simulated annealing structure solution, using *DSS* and profile intensity data in the 2θ range 10–50°, consisted of the four Ca atoms and the two SiO_4 tetrahedra in the asymmetric unit, all of which were located at general equivalent positions. The four Ca atoms were treated as independent atoms, each of which had variable fractional coordinates of x, y and z. On the other hand, the SiO_4 tetrahedra were treated as rigid molecules having a regular tetrahedral shape and an Si—O distance of 1.64 Å. The SiO_4 molecule was translated and rotated around the rotation axis through the centre of gravity of the molecule (atomic position of Si). The variable parameters for each SiO_4 tetrahedron were the x, y and z coordinates for the centre of gravity, rotation angle ψ, and θ and φ angles for representing the direction of the rotation axis in the polar coordinate system. In each cycle of simulated annealing, 24 variable parameters, in total, were varied simultaneously for Monte Carlo moves within a space of the unit cell. Profile parameters, such as the U, V and W parameters in the Caglioti *et al.* (1958) formula, were employed from those refined with *WPPF*. Only a scale factor was refined in each simulated annealing cycle. The objective function used was the conventional R_{wp} factor for profile intensities (Young, 1995). The so-called temperature parameter in simulated annealing was decreased following the scheme defined by $T_{i+1} = \rho T_i$, where T_i and T_{i+1} are the temperatures in the ith and $(i + 1)$th cycles, respectively, and ρ is the tuning parameter (Kirkpatrick *et al.*, 1983). A re-annealing technique was used in order to avoid falling into traps of local minima (Ingber, 1989), and it was demonstrated to operate very effectively. A solution with an R_{wp} factor of 30.3% was obtained after 40000 simulated annealing cycles. A decrease of the maximum displacement for the Monte Carlo moves further reduced the R_{wp} factor to 25.2%. The solution proved to be a correct structural solution in the subsequent Rietveld refinement.

4. Rietveld refinement

A profile intensity data set having a 2θ range 10–155° was used for Rietveld refinement (Rietveld, 1969) with the computer program *PFLS* (version 5.00) (Toraya, 2000). It contained very weak reflections (2θ range = 32.3–32.8°) from the β-C_2S as a coexisting impurity. Therefore, the two phases, x-C_2S (1674 independent reflections) and β-C_2S (722 independent reflections), were assumed to be present in the Rietveld refinement.

The split-type pseudo-Voigt function was used for representing the profile shape. The refined profile parameters were six background parameters in the fifth-degree polynomial background function, the unit-cell parameters, the 2θ-zero

Table 2
Selected interatomic distances (Å) and bond angles (°) of x-C_2S.

Numbers in parentheses represent the estimated statistical uncertainties.

$Ca(1)O_6$		$Ca(2)O_7$	
Ca(1)—O(1)^{i}	2.247 (6)	Ca(2)—O(1)	2.330 (6)
Ca(1)—O(2)	2.347 (7)	Ca(2)—O(2)	2.900 (7)
Ca(1)—O(3)^{iv}	2.699 (7)	Ca(2)—O(4)^{ii}	2.397 (6)
Ca(1)—O(3)^{iii}	2.283 (6)	Ca(2)—O(5)	2.441 (6)
Ca(1)—O(5)	2.250 (7)	Ca(2)—O(7)^{iii}	2.417 (5)
Ca(1)—O(6)^{v}	2.409 (7)	Ca(2)—O(8)	2.438 (6)
		Ca(2)—O(8)^{ii}	2.418 (7)
Average Ca(1)—O	2.373	Average Ca(2)—O	2.477
O(1)^{i}—O(2)	3.018 (9)	O(1)—O(2)	2.619 (10)
O(1)^{i}—O(3)^{iv}	2.582 (9)	O(1)—O(4)^{ii}	3.120 (8)
O(1)^{i}—O(5)	3.771 (9)	O(1)—O(7)^{iii}	3.430 (8)
O(1)^{i}—O(6)^{v}	3.553 (8)	O(1)—O(8)^{ii}	3.155 (8)
O(2)—O(3)^{iv}	3.863 (10)	O(2)—O(4)^{ii}	3.464 (8)
O(2)—O(3)^{iii}	3.250 (8)	O(2)—O(5)	3.303 (9)
O(2)—O(5)	3.303 (9)	O(4)^{ii}—O(8)	3.119 (8)
O(3)^{iv}—O(3)^{iii}	3.419 (8)	O(4)^{ii}—O(8)^{ii}	3.372 (8)
O(3)^{iv}—O(6)^{v}	3.168 (9)	O(5)—O(7)^{iii}	3.222 (8)
O(3)^{iii}—O(5)	3.477 (9)	O(5)—O(8)	2.713 (9)
O(3)^{iii}—O(6)^{v}	3.215 (9)	O(7)^{iii}—O(8)	3.765 (7)
O(5)—O(6)^{v}	3.368 (9)	O(7)^{iii}—O(8)^{ii}	3.143 (8)
		O(8)—O(8)^{ii}	3.191 (8)
Average O—O	3.332	Average O—O	3.201

$Ca(3)O_7$		$Ca(4)O_8$	
Ca(3)—O(3)^{ix}	3.047 (6)	Ca(4)—O(1)^{i}	2.173 (7)
Ca(3)—O(4)^{i}	2.422 (6)	Ca(4)—O(2)	3.029 (5)
Ca(3)—O(5)	2.491 (6)	Ca(4)—O(2)^{vi}	2.255 (6)
Ca(3)—O(6)	2.382 (6)	Ca(4)—O(3)^{vii}	2.348 (7)
Ca(3)—O(7)^{v}	2.378 (7)	Ca(4)—O(4)^{xi}	3.164 (7)
Ca(3)—O(7)^{iii}	3.033 (6)	Ca(4)—O(4)^{viii}	2.773 (6)
Ca(3)—O(8)^{iii}	2.368 (6)	Ca(4)—O(6)^{iii}	2.310 (8)
		Ca(4)—O(8)^{iii}	3.031 (6)
Average Ca(3)—O	2.589	Average Ca(4)—O	2.635
O(3)^{ix}—O(4)^{i}	2.792 (8)	O(1)^{i}—O(2)	3.018 (9)
O(3)^{ix}—O(6)	3.215 (9)	O(1)^{i}—O(4)^{xi}	2.690 (8)
O(3)^{ix}—O(7)^{v}	3.721 (9)	O(1)^{i}—O(4)^{viii}	3.120 (8)
O(4)^{i}—O(6)	4.206 (7)	O(1)^{i}—O(8)^{iii}	3.155 (8)
O(4)^{i}—O(7)^{v}	3.465 (8)	O(2)—O(3)^{vii}	2.650 (8)
O(4)^{i}—O(7)^{iii}	4.383 (8)	O(2)—O(4)^{xi}	4.224 (9)
O(4)^{i}—O(8)^{iii}	3.119 (8)	O(2)—O(6)^{iii}	4.130 (8)
O(5)—O(6)	2.503 (10)	O(2)—O(8)^{iii}	4.493 (8)
O(5)—O(7)^{v}	3.366 (8)	O(2)^{vi}—O(3)^{vii}	3.250 (8)
O(5)—O(7)^{iii}	3.222 (8)	O(2)^{vi}—O(4)^{xi}	3.464 (8)
O(5)—O(8)^{iii}	3.563 (7)	O(2)^{vi}—O(4)^{viii}	2.692 (9)
O(6)—O(7)^{iii}	3.936 (8)	O(2)^{vi}—O(6)^{iii}	3.407 (10)
O(7)^{v} —O(8)^{iii}	3.143 (8)	O(3)^{vii}—O(4)^{xi}	4.160 (9)
O(7)^{iii}—O(8)^{iii}	2.683 (9)	O(3)^{vii}—O(6)^{iii}	3.168 (9)
		O(4)^{xi}—O(4)^{viii}	3.726 (8)
		O(4)^{viii}—O(6)^{iii}	3.835 (9)
		O(4)^{viii}—O(8)^{iii}	3.372 (8)
		O(6)^{iii}—O(8)^{iii}	2.591 (9)
Average O—O	3.380	Average O—O	3.397

$Si(1)O_4$		$Si(2)O_4$	
Si(1)—O(1)^{x}	1.582 (7)	Si(2)—O(5)	1.628 (7)
Si(1)—O(2)^{x}	1.627 (7)	Si(2)—O(6)	1.597 (8)
Si(1)—O(3)	1.636 (6)	Si(2)—O(7)	1.569 (6)
Si(1)—O(4)	1.697 (6)	Si(2)—O(8)	1.658 (7)
Average Si(1)—O	1.636	Average Si(2)—O	1.613
O(1)^{x}—O(2)^{x}	2.619 (10)	O(5)—O(6)	2.503 (10)
O(1)^{x}—O(3)	2.582 (9)	O(5)—O(7)	2.648 (7)
O(1)^{x}—O(4)	2.690 (8)	O(5)—O(8)	2.713 (9)
O(2)^{x}—O(3)	2.650 (8)	O(6)—O(7)	2.648 (8)
O(2)^{x}—O(4)	2.692 (9)	O(6)—O(8)	2.591 (9)
O(3)—O(4)	2.792 (8)	O(7)—O(8)	2.683 (9)
Average O—O	2.671	Average O—O	2.631
O(1) ^{x}—Si(1)—O(2)^{x}	109.4 (4)	O(5)—Si(2)—O(6)	101.8 (3)
O(1)^{x}—Si(1)—O(3)	106.7 (4)	O(5)—Si(2)—O(7)	111.8 (4)
O(1)^{x}—Si(1)—O(4)	110.2 (4)	O(5)—Si(2)—O(8)	111.3 (3)
O(2)^{x}—Si(1)—O(3)	108.6 (4)	O(6)—Si(2)—O(7)	113.5 (3)
O(2)^{x}—Si(1)—O(4)	108.1 (3)	O(6)—Si(2)—O(8)	105.5 (4)
O(3)—Si(1)—O(4)	113.8 (3)	O(7)—Si(2)—O(8)	112.4 (3)
Average O—Si(1)—O	109.5	Average O—Si(2)—O	109.4

Symmetry codes: (i) $x, \frac{1}{2}-y, \frac{1}{2}+z$; (ii) $1-x, 1-y, 1-z$; (iii) $1-x, \frac{1}{2}+y, \frac{1}{2}-z$; (iv) $1+x, \frac{1}{2}-y, -\frac{1}{2}+z$; (v) $1-x, 1-y, -z$; (vi) $2-x, -\frac{1}{2}+y, \frac{1}{2}-z$; (vii) $1+x, y, z$; (viii) $1-x, -\frac{1}{2}+y, -\frac{1}{2}-z$; (ix) $x, \frac{1}{2}-y, -\frac{1}{2}+z$; (x) $-1+x, y, z$; (xi) $1+x, \frac{1}{2}-y, \frac{1}{2}+z$.

point, the U, V and W parameters, four η parameters on the low- and high-angle sides of the peak, four coefficients in the function of symmetrized harmonic expansion for preferred orientation correction (Järvinen, 1993), and the scale factors for the x-C_2S and β-C_2S phases. All structural parameters (x, y and z) for 14 atoms in an asymmetric unit of the x-C_2S were refined simultaneously together with the profile parameters, whereas those for β-C_2S were fixed at values given by Jost *et al.* (1977). Isotropic displacement parameters for individual atoms ($U_{\rm iso}^{\rm individ}$) were fixed at values that were obtained by averaging literature values for each kind of atom of α-C_2SH (Yano *et al.*, 1993), and an overall displacement parameter $U_{\rm iso}^{\rm overall}$ was refined instead. All parameters were smoothly converged in the least-squares refinement using the weight function in the form $w_i = 1/Y_{oi}$ (where Y_{oi} is the observed profile intensity at the ith step). The final reliability indices were $R_{wp} = 11.6\%$, $R_p = 8.44\%$ and goodness-of-fit = 2.28 for the whole powder pattern, $R_{\rm Bragg} = 6.97\%$ and $R_F = 5.77\%$ for x-C_2S, and $R_{\rm Bragg} = 14.7\%$ and $R_F = 8.64\%$ for β-C_2S.

The weight ratio of x-C_2S to β-C_2S, derived from the refined scale factors, was 0.965:0.035. Factors for the preferred orientation correction (applied only to x-C_2S) were in the range from 0.65 (h00) to 1.60 (0k0), indicating the presence of a rather strong preferred orientation along the plane normal of plate-like crystallites of x-C_2S. A fitting result of the Rietveld refinement is shown in Fig. 2. Selected interatomic distances and bond angles of x-C_2S are given, together with symmetry codes, in Table 2.[1]

Atomic scattering factor tables used in the present study for neutral atoms were taken from *International Tables for X-ray Crystallography* (1974, Vol. IV).

5. Results and discussion

5.1. Crystal structure of x-C_2S

The crystal structure of x-C_2S, shown in Fig. 3, consists of isolated SiO_4 tetrahedra and a three-dimensional CaO_n polyhedral network. If O atoms within a distance of 3.2 Å are

[1] Supplementary data for this paper are available from the IUCr electronic archives (Reference: CK0012). Services for accessing these data are described at the back of the journal.

counted as coordinated to the Ca atoms, $n = 6$ for Ca(1), $n = 7$ for Ca(2) and Ca(3), and $n = 8$ for Ca(4). The Ca(4)—O(4)^{xi} distance of 3.164 (7) Å is rather long compared with the remaining Ca—O distances. However, much longer Ca—O distances of 3.18 Å to 3.34 Å will be found in α'_L-C_2S, which is the high-temperature form of x-C_2S (Udagawa *et al.*, 1979). Valence sums V [$V = \sum s_i$, where s_i is the bond strength defined by Brown & Shannon (1973)], calculated for x-C_2S, were 2.4, 1.9, 1.9, 1.6, 1.9, 2.1, 1.8 and 1.9 for atoms O(1) to O(8), respectively; they were slightly larger than the average for O(1) and smaller for O(4). Although the contribution of the Ca(4)—O(4)^{xi} bond to V is not large, it was concluded that O(4)^{xi} should be included as coordinated to the Ca(4) atom. α-C_2SH, from which x-C_2S was formed at temperatures of 663–763 K, has two $Ca(O,OH)_6$ polyhedra and another two $Ca(O,OH)_7$ polyhedra (Yano *et al.*, 1993). On the other hand, α'_L-C_2S has much higher coordination numbers of eight to ten for the Ca atoms (Udagawa *et al.*, 1979). The average of all Ca—O distances in x-C_2S (2.53 Å) is also in between those in α-C_2SH (2.45 Å) and α'_L-C_2S (2.64 Å). The increase/decrease in the coordination number and the Ca—O distance compared with those of lower/higher temperature forms are well in accordance with a general trend observed in the C_2S family.

In Table 2, O—O edges with lengths of <3 Å in CaO_n polyhedra are all shared with one of the two SiO_4 tetrahedra in the asymmetric unit. All six edges of $Si(1)O_4$ are shared with neighbouring CaO_n polyhedra, while the number of shared edges is four in $Si(2)O_4$. Inter-Ca—Si distances of 2.96–3.25 Å, calculated from positional parameters, agree well with those of 2.91–3.22 Å estimated from a geometrical model. These distances, together with close inspection of a three-dimensional graphic display of the structure, confirm that the sharing style between the CaO_n and SiO_4 polyhedra is the edge share. The $Si(1)O_4$ tetrahedron is larger than the $Si(2)O_4$ tetrahedron because of the greater number of shared edges and, therefore, greater repulsive Coulomb force between the Ca and Si atoms.

The crystal structure of x-C_2S viewed along the c axis and that of α-C_2SH along the a axis (Yano *et al.*, 1993) are shown in Fig. 4. We can see that tunnels having similar sizes and shapes are running in the direction perpendicular to the two diagrams. As will be discussed in §5.2, x-C_2S and α-C_2SH have an axial relationship in their unit-cell parameters, and these

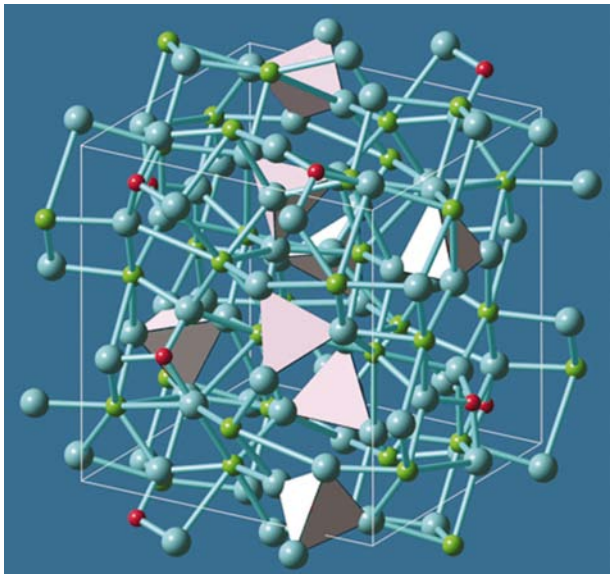

Figure 3
Crystal structure of x-C_2S. Green spheres: Ca; red spheres: Si; light blue spheres: O. Tetrahedra represent eight SiO_4 molecules inside the unit cell.

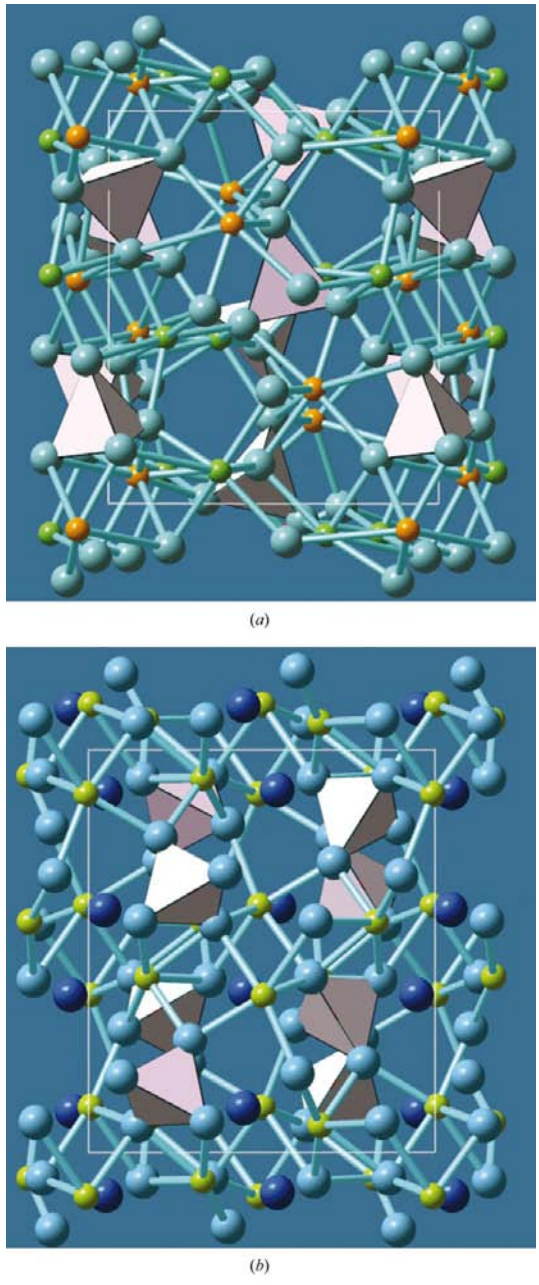

Figure 4
Crystal structures of x-C_2S and α-C_2SH, viewed along (*a*) the c axis of x-C_2S and (*b*) the a axis of α-C_2SH. Tunnels with pentagonal-shaped sections run perpendicular to the diagrams. Orange spheres in x-C_2S represent Ca(3) and Ca(4) atoms, belonging to the group of large polyhedra (G_L) (§5.3.2). Blue spheres in α-C_2SH represent hydroxyls. The other spheres represent respective atoms as in Fig. 3.

Table 3
Distances (Å) from Si atoms in x-C_2S to the nearest-neighbour Si atoms in α-C_2SH.

The axial setting of the unit-cell is changed, and atoms in x-C_2S are translated by operations described in §5.2.2. ΔX, ΔY and ΔZ represent component distances along the a, b and d_{001} axes of x-C_2S, respectively. Symmetry codes for Si atoms in x-C_2S are in accordance with those given in Table 2. Symmetry codes for α-C_2SH, belonging to the space group $P2_12_12_1$, are given by (i) $\frac{1}{2}-x$, $-y$, $\frac{1}{2}+z$; (ii) $\frac{1}{2}+x$, $\frac{1}{2}-y$, $-z$; (iii) $-x$, $\frac{1}{2}+y$, $\frac{1}{2}-z$. Atomic parameters of Si atoms in α-C_2SH were taken from those given by Yano *et al.* (1993).

Atoms in x-C_2S	Atoms in α-C_2SH	Distance	ΔX	ΔY	ΔZ
Si(1)	Si(2)^{ii}	2.53	0.47	2.23	−1.09
Si(1)^{i}	Si(1)^{i}	1.12	−0.00	−0.60	−0.95
Si(1)^{ii}	Si(1)	0.87	−0.26	0.80	0.22
Si(1)^{iii}	Si(2)^{iii}	0.25	0.09	−0.21	0.08
Si(2)	Si(1)^{ii}	2.32	0.37	−2.28	−0.14
Si(2)^{i}	Si(2)^{i}	3.04	−0.10	3.04	0.00
Si(2)^{ii}	Si(1)^{iii}	3.53	−0.22	3.39	0.94
Si(2)^{iii}	Si(2)	2.11	0.25	−1.93	0.81
Averages		1.97			

tunnels run in the common axial direction. In α-C_2SH, the tunnels are sandwiched between the two-dimensional $Ca(O,OH)_n$ polyhedral network planes parallel to (001), and all hydroxyls (blue spheres in Fig. 4*b*) face the tunnels, which may be used as paths for hydroxyls/water molecules during dehydration.

5.2. Structural change from α-C_2SH to x-C_2S

5.2.1. Presence of pseudo-glide plane in α-C_2SH. All atoms in α-C_2SH, which belongs to the space group $P2_12_12_1$, are related by twofold screw axes (Yano *et al.*, 1993). Now let us disregard discrimination between the atoms of the same kind but belonging to different asymmetric units. Then we can see that positions for most of the atoms in α-C_2SH can approximately be related to the pseudo-*a* glide planes, which are supposed to be present perpendicular to the *c* axis. Differences between the actual atomic position and the position generated by symmetry operation of the *a*-glide plane for the same kind of atoms are just ∼0.01 in fractional coordinates. Only two O atoms and two hydroxyls [O(1) at $\frac{1}{2}+x, 1-y, 1-z$; O(2) at $1-x, \frac{1}{2}+y, \frac{1}{2}-z$; O(9) at x, y, z; and O(10) at $\frac{1}{2}-x, \frac{1}{2}-y, \frac{1}{2}+z$ in notation for atoms given by Yano *et al.* (1993)] among the 64 atoms in the unit cell apparently deviate (>0.01) from the equivalent positions of the *a*-glide plane. The pseudo-*a*-glide plane corresponds to the *c*-glide plane in x-C_2S on the assumed relationship in the unit-cell parameter of $a_\alpha \rightarrow c_x$, $b_\alpha \rightarrow d_{100x}$ and $c_\alpha \rightarrow b_x$ between the two forms (Miyazaki *et al.*, 1998). A selected-area electron diffraction pattern of the *hk*0 reciprocal plane of α-C_2SH [Fig. 2(*d*) in Miyazaki *et al.* (1998)] also confirms the presence of the pseudo-glide plane: the intensities of reflections having indices of *hk*0 with $h = 2n+1$ are systematically very weak compared with those with $h = 2n$. Here it may be pointed out that the symbols a^* and b^* used for representing the reciprocal axes in Fig. 2(*d*) of Miyazaki *et al.* (1998) were mistakenly exchanged with each other.

5.2.2. Displacement of SiO_4 tetrahedra. The crystal structure of x-C_2S, projected along the *a* and *b* axes, and that of α-C_2SH, along the *b* and *c* axes, are shown in Fig. 5. The structures of x-C_2S and α-C_2SH, when viewed along the *b* axis of x-C_2S (Fig. 5*a*) and the *c* axis of α-C_2SH (Fig. 5*b*), have a close resemblance regarding the dispositions of SiO_4 tetrahedra. On the other hand, their difference is very clear when Fig. 5(*c*) (x-C_2S along the *a* axis) and Fig. 5(*d*) (α-C_2SH along the *b* axis) are compared with each other. Then the crystal structure of x-C_2S was superimposed on the structure of α-C_2SH by giving the orientation relationship of $a_\alpha = c_x$, $b_\alpha = d_{100x}$ and $c_\alpha = b_x$ (§5.2.1). The structure of x-C_2S was further translated by distances of −3.27, 4.34 and 3.71 Å along the a_α, b_α and c_α axes, respectively, in order to obtain the closest approach of Si atoms between the two structures. The relative distances between the two neighbouring Si atoms, one belonging to x-C_2S and the other to α-C_2SH, are given in Table 3. In their calculation, thermal expansion of the unit cell of x-C_2S at elevated temperatures and shrinkage of the unit cell of α-C_2SH during the dissociation process were ignored. The SiO_4 tetrahedra are supposed to behave as rigid molecules during the dissociation process. They would be displaced primarily along the direction of the *c* axis in α-C_2SH (the *b* axis in x-C_2S), and undergo some degree of rotation, in order to fill the space induced by the dehydration of α-C_2SH (Fig. 5 and Table 3). It should be noted that two SiO_4 tetrahedra [Si(1)^{iii} and Si(2)^{i} in α-C_2SH] and their counterparts [Si(1)^{ii} and Si(2)] are largely displaced by ∼2 Å to 3 Å in the opposite directions

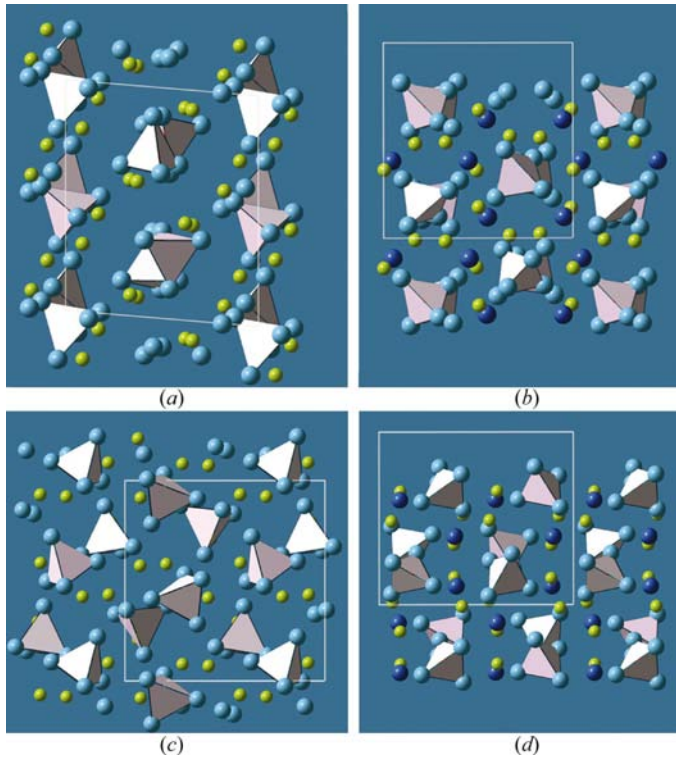

Figure 5
Crystal structures of x-C_2S and α-C_2SH, viewed along (*a*) the *b* axis of x-C_2S, (*b*) the *c* axis of α-C_2SH, (*c*) the *a* axis of x-C_2S and (*d*) the *b* axis of α-C_2SH. Arrows in (*d*) represent displacements of SiO_4 tetrahedra, expected from a comparison of both structures. Spheres represent respective atoms as in Figs. 3 and 4.

Table 4
Ratios (%) of the number of edges shared between the Ca—Ca and Ca—Si polyhedra to the total number of edges in x-C_2S and related compounds.

		α-C_2SH	γ-C_2S	x-C_2S	α'_L-C_2S
CaO_n	Ca—Ca	32.0	25.0	42.1	63.4
	Ca—Si	6.0	12.5	17.5	17.9
	Total	38.0	37.5	59.6	81.3
SiO_4	Ca—Si	25.0	50.0	83.3	83.3

from each other along the c axis of α-C_2SH (arrows in Fig. 5d). The SiO_4 tetrahedra in α-C_2SH are displaced as if the pseudo-a-glide plane, which is taken over as the c-glide plane in x-C_2S, governs them.

5.2.3. CaO_n polyhedral networks. Ratios (in %) of the number of shared edges to the total number of edges of CaO_n and SiO_4 polyhedra are given for x-C_2S, α-C_2SH, α'_L-C_2S and γ-C_2S in Table 4. In the crystal structure of α-C_2SH, the two-dimensional $Ca(O,OH)_n$ polyhedral network planes run parallel to (001) (Yano *et al.*, 1993), and they are connected vertically with rows of the SiO_4 tetrahedra, running parallel to the c axis (Fig. 4b). Therefore, only a quarter of the edges of the SiO_4 tetrahedra are shared with the two $Ca(O,OH)_7$ polyhedra. By reflecting such a structural feature of α-C_2SH, the average ratio of shared edges for $Ca(O,OH)_n$ polyhedra is just 38%. On the other hand, the SiO_4 tetrahedra in x-C_2S are surrounded by CaO_n polyhedra composing the three-dimensional network as shown in Fig. 3 (§5.1), and the ratio of shared edges is ~60%.

Relative distances from one Ca atom in α-C_2SH to the nearest-neighbour Ca atom in x-C_2S, calculated by the same scheme as described in §5.2.2, are in the range 1.0 Å to 2.7 Å, giving an average distance of 1.96 Å. The components of the average relative distances between the two Ca atoms along the directions of the a_α, b_α and c_α axes are 1.1, 0.6 and 1.1 Å, respectively. Structural change of the polyhedral network from two-dimensions to three-dimensions in α-$C_2SH \rightarrow x$-C_2S will be associated with the large displacements of the SiO_4 tetrahedra in the direction perpendicular to the two-dimensional polyhedral network in α-C_2SH (Figs. 4 and 5).

5.3. Structural change from x-C_2S to α'_L-C_2S

5.3.1. Size gaps between the CaO_n and SiO_4 polyhedra. The crystal structures of the five C_2S polymorphs that have been known up to the present are classified into two structural types. One is the olivine-type, to which the γ-form belongs, and the other is the β-K_2SO_4-type, to which the remaining four high-temperature forms of α, α'_H, α'_L and β belong (Udagawa, 1980). The crystal structure of α'_L-C_2S is a superstructure of the β-K_2SO_4-type, and it has an orthorhombic unit cell with dimensions of a = 6.812(3)×3, b = 9.339 (2) and c = 5.553 (2) Å, containing 12 units of chemical formula Ca_2SiO_4 (Udagawa *et al.*, 1979). It is well known that the olivine-type and β-K_2SO_4-type structures can be derived from the hexagonal closest packing (h.c.p.) of O atoms (Bragg & Claringbull, 1965). In ideal geometry, 16 octahedral sites and 32 tetrahedral sites are available for unit cells of the olivine-type and β-K_2SO_4-type structures (the number of chemical formula unit = 4 in this case). In γ-C_2S, the Ca atoms occupy half of the available octahedral sites, while the shapes of the CaO_6 octahedra are largely distorted because of the small size of the SiO_4 tetrahedra compared with that in the ideal h.c.p. geometry. With increasing temperature, the size of the CaO_n polyhedra is greatly increased by thermal expansion while the size of the SiO_4 tetrahedra is almost unchanged (Smyth & Hazen, 1973). In the crystal structures of the high-temperature forms in the C_2S family, the size differences between the CaO_n and SiO_4 polyhedra at the formation temperatures of these forms become much greater than those in the γ-form. Therefore, in α'_L-C_2S, half of the Ca atoms in the unit cell occupy tenfold coordination sites as in the case of β-K_2SO_4 (McGinnety, 1972). In this case, just four octahedral sites in a sub-cell unit (12 octahedral sites in a super-lattice of α'_L-C_2S) are left for the remaining half of Ca atoms. The sixfold coordination sites are, however, intolerably small for the large Ca atoms, and SiO_4 tetrahedra are shifted, rotated and distorted in order to squeeze the Ca atoms into these sites. Then the coordination number for these sites is increased to sevenfold to ninefold, and is eightfold in the case of α'_L-C_2S.

5.3.2. CaO_n polyhedral networks in x-C_2S to α'_L-C_2S. CaO_n polyhedra in dicalcium silicates can be divided evenly, according to their sizes, into two groups, G_S (small polyhedra) and G_L (large polyhedra). Classification of the CaO_n polyhedra in x-C_2S and α'_L-C_2S into the two groups is given in Table 5, together with information about the first-neighbour CaO_n polyhedra around the individual CaO_n polyhedra. Firstly, we can see that the size difference between the two groups is increased by increasing the transformation temperature of individual phases: the differences in the average Ca—O distance between the two groups G_S and G_L are 0.03 Å in the room-temperature form of γ-C_2S (Udagawa *et al.*, 1980), 0.07 Å in α-C_2SH (Yano *et al.*, 1993), 0.19 Å in x-C_2S and 0.27 Å in α'_L-C_2S (Udagawa *et al.*, 1979). Secondly, in both structures of x-C_2S and α'_L-C_2S, smaller CaO_n polyhedra are surrounded primarily by larger ones, and *vice versa* for larger polyhedra (Table 5). For example, a small $Ca(1)O_6$ polyhedron in x-C_2S is surrounded by five large CaO_n polyhedra (orange spheres in Fig. 4a) and three small ones (green spheres). In the case of α'_L-C_2S, a small $Ca(4)O_8$ polyhedron is surrounded by six large polyhedra and only two small ones. Such an alternate arrangement of large and small CaO_n polyhedra in x-C_2S and α'_L-C_2S will achieve denser packing than expanding evenly all the CaO_n polyhedra, and it may be thermally more stable.

5.3.3. Structural change from x-C_2S to α'_L-C_2S. The large gap between the available polyhedral space and the actual size of CaO_n polyhedra at high temperatures will be a cause for inducing the transformation from x-C_2S to α'_L-C_2S. With elevating the temperature above 1193 K, $Ca(1)O_6$ and $Ca(2)O_7$ polyhedra in x-C_2S are supposed to change the coordination number to eightfold, and $Ca(3)O_7$ and $Ca(4)O_8$ to tenfold. The SiO_4 tetrahedra will again behave like rigid molecules, and the rotations of SiO_4 tetrahedra will achieve

Table 5
The numbers of first-neighbour CaO_n polyhedra around respective CaO_n polyhedra.

Inter Ca—Ca distances were all within 43 Å. Notation for atoms in α'_L-C_2S given by Udagawa *et al.* (1979) is used.

			G_S		G_L	
x-C_2S		Average Ca—O	Ca(1)	Ca(2)	Ca(3)	Ca(4)
G_S	Ca(1)	2.373	1	2	2	3
	Ca(2)	2.477	2	1	3	2
G_L	Ca(3)	2.589	2	3	0	1
	Ca(4)	2.635	3	2	1	0

α'_L- C_2S			Ca(4)	Ca(5)	Ca(6)	Ca(1)	Ca(2)	Ca(3)
G_S	Ca(4)	2.495	0	1	1	0	3	3
	Ca(5)	2.500	1	0	1	3	2	1
	Ca(6)	2.513	1	1	0	3	1	2
G_L	Ca(1)	2.775	0	3	3	0	2	0
	Ca(2)	2.757	3	2	1	2	0	0
	Ca(3)	2.781	3	1	2	0	0	2

the change of the coordination number of CaO_n polyhedra. In x-C_2S, as has been mentioned in §5.1, the $Si(1)O_4$ and $Si(2)O_4$ tetrahedra have six and four shared edges with CaO_n polyhedra, respectively. In α'_L-C_2S, three kinds of SiO_4 tetrahedra in the asymmetric unit equally share one face, three edges and one corner with neighbouring CaO_n polyhedra just as in the β-K_2SO_4-type structure. The small tunnel space around the $Si(2)O_4$ tetrahedra in x-C_2S is collapsed in α'_L-C_2S. Then the ratio of shared edges for Ca—Ca is increased by ~20% in α'_L-C_2S (Table 4), and the edges of nearly 80% of CaO_n polyhedra are shared with surrounding polyhedra. Accompanied by this structural change, the density of α'_L-C_2S is increased by 0.3 g cm^{-3} compared with that of x-C_2S.

Both x-C_2S and γ-C_2S are directly transformed into α'_L-C_2S. However, the transformation temperature for x-C_2S is ~373 K higher than that for γ-C_2S, in which all Ca atoms are in the sixfold coordination. Both transformations are irreversible, and α'_L-C_2S is always transformed into β-C_2S when it is cooled (Fig. 1). A reason for these irreversible transformations may be structural affinity in that β-C_2S belongs to the same β-K_2SO_4-type structure as α'_L-C_2S.

6. Summary

The new phase of dicalcium silicate, x-C_2S, was formed by heating α-C_2SH at temperatures of ~663–763 K, and it was transformed into α'_L-C_2S above ~1193 K (Ishida *et al.*, 1993) (Fig. 1). Its crystal structure has been determined by simulated annealing and refined by the Rietveld method using synchrotron radiation powder diffraction data. In α-C_2SH, the $Ca(O,OH)_n$ polyhedra constitute the two-dimensional polyhedral networks, and the isolated SiO_4 tetrahedra connect the networks three-dimensionally. The small tunnels run parallel to the network planes, and they are supposed to be used for passing hydroxyls/water molecules during dehydration. In order to fill the space induced by dehydration, the SiO_4 tetrahedra are largely displaced in the direction perpendicular to the network planes. The Ca atoms are also displaced, and their coordination is rearranged, forming the three-dimensional CaO_n network in x-C_2S. The isolated SiO_4 tetrahedra and the three-dimensional network are common structural features observed in all members of the C_2S family.

The crystal structures of α'_L-C_2S and the remaining three high-temperature forms of α, α'_H and β belong to the β-K_2SO_4-type. Dispositions of the SiO_4 and CaO_n polyhedra in x-C_2S are similar to those in α'_L-C_2S, and large and small CaO_n polyhedra are alternately arranged in both structures. However, the SiO_4 tetrahedra in x-C_2S share only their edges with neighbouring CaO_n polyhedra, whereas the SiO_4 tetrahedra in α'_L-C_2S share also their corners and faces. The crystal structure of x-C_2S also differs from the olivine-type, to which the γ-C_2S belongs, and, therefore, it forms a new structural type in the C_2S family. With elevating temperatures, the sizes of the CaO_n polyhedra in x-C_2S become too large to confine the Ca atoms in the sixfold to eightfold coordination, and the Ca atoms take the eightfold to tenfold coordination in α'_L-C_2S. α'_L-C_2S is further transformed into β-C_2S on subsequent cooling. The structures of α'_L-C_2S and β-C_2S are based on the same structural type of β-K_2SO_4, and structural affinity of these structures may be a reason why the transformation of x-C_2S to α'_L-C_2S is irreversible.

The present study is financially supported by the Ministry of Education, Science, Sports and Culture (Grant-in-Aid for Exploratory Research, 12875123).

References

Bragg, L. & Claringbull, G. F. (1965). *Crystal Structures of Minerals*, pp. 96–99 and pp. 173–175. London: Bell.
Brown, I. D. & Shannon, R. D. (1973). *Acta Cryst.* A**29**, 266–282.
Caglioti, G., Paoletti, A. & Ricci, F. P. (1958). *Nucl. Instrum.* **3**, 223–228.
Catti, M., Gazzoni, G. & Ivaldi, G. (1984). *Acta Cryst.* B**40**, 537–544.
Czaya, R. (1971). *Acta Cryst.* B**27**, 848–849.
Eysel, W. & Hahn, T. (1970). *Z. Kristallogr.* **131**, 322–341.
Il'inets, A. M. & Bikbau, M. Ya. (1990). *Sov. Phys. Crystallogr.* **35**, 54–56.
Ingber, L. (1989). *Math. Comput. Model.* **12**, 967–973.
Ishida, H., Yamazaki, S., Sasaki, K., Okada, Y. & Mitsuda, T. (1993). *J. Am. Ceram. Soc.* **76**, 1707–1712.
Järvinen, M. (1993). *J. Appl. Cryst.* **26**, 525–531.
Jost, K. H., Ziemer, B. & Seydel, R. (1977). *Acta Cryst.* B**33**, 1696–1700.
Kirkpatrick, S., Gelatt, C. D. Jr & Vecchi, M. P. (1983). *Science*, **220**, 671–680.
Kriven, W. M. (1988). *J. Am. Ceram. Soc.* **71**, 1021–1030.
McGinnety, J. A. (1972). *Acta Cryst.* B**28**, 2845–2852.
Midgley, C. M. (1952). *Acta Cryst.* **5**, 307–312.
Miyazaki, M., Yamazaki, S., Sasaki, K., Ishida, H. & Toraya, H. (1998). *J. Am. Ceram. Soc.* **81**, 1339–1343.
Mumme, W. G., Hill, R. J., Bushnell-Wye, G. & Segnit, E. R. (1995). *N. Jahrb. Mineral. Abh.* **169**, 35–68.

Pawley, G. S. (1981). *J. Appl. Cryst.* **14**, 357–361.
Rasberry, S. D. (1987). *NIST* Certificate for SRM640*b* Si powder.
Rietveld, H. M. (1969). *J. Appl. Cryst.* **2**, 65–71.
Smith, D. K., Majumdar, A. & Ordway, F. (1965). *Acta Cryst.* **18**, 787–795.
Smyth, J. R. & Hazen, R. M. (1973). *Am. Mineral.* **58**, 588–593.
Toraya, H. (1986). *J. Appl. Cryst.* **19**, 440–447.
Toraya, H. (2000). *J. Appl. Cryst.* **33**, 95–102.
Toraya, H., Hibino, H. & Ohsumi, K. (1996). *J. Synchrotron Rad.* **3**, 75–83.
Udagawa, S. (1980). *Proc. Gen. Meet. Cem. Assoc. Jpn*, **34**, 31–39. (In Japanese.)
Udagawa, S. & Urabe, K. (1978). *Proc. Gen. Meet. Cem. Assoc. Jpn*, **32**, 35–38. (In Japanese.)
Udagawa, S., Urabe, K., Natsume, M. & Yano, T. (1980). *Cem. Concr. Res.* **10**, 139–144.
Udagawa, S., Urabe, K., Yano, T., Takada, K. & Natsume, M. (1979). *Proc. Gen. Meet. Cem. Assoc. Jpn*, **33**, 35–38. (In Japanese.)
Visser, J. W. (1969). *J. Appl. Cryst.* **2**, 89–95.
Yamazaki, S. & Toraya, H. (2001). *Powder Diffr.* **16**, 110–114.
Yano, T., Urabe, K., Ikawa, H., Teraushi, T., Ishizawa, N. & Udagawa, S. (1993). *Acta Cryst.* C**49**, 1555–1559.
Young, R. A. (1995). *The Rietveld Method*, pp. 1–38. Oxford University Press.